Available online at www.sciencedirect.com
SCIENCE DIRECT®
Journal of Power Sources 142 (2005) 279–284
JOURNAL OF POWER SOURCES
www.elsevier.com/locate/jpowsour

Structure and electrochemistry of $FePO_4 \cdot 2H_2O$ hydrate

K. Zaghib[a,*], C.M. Julien[b]

[a] *Institut de Recherche d'Hydro-Québec, 1800 Boulevard Lionel-Boulet, Varennes, Que., Canada J3X 1S1*
[b] *Laboratoire des Milieux Désordonnés et Hétérogènes, CNRS-UMR 7603, Université Pierre et Marie Curie, 140 rue de Lourmel, 75015 Paris, France*

Received 5 September 2004; accepted 30 September 2004
Available online 29 December 2004

Abstract

We report the structural and electrochemical characteristics of $FePO_4$ dihydrate exhibiting a monoclinic structure ($P2_1/n$ space group). We have applied Raman and FTIR spectroscopy to study the local structure. Vibrational features analyzed using the molecular group model show the strong inductive effect in the [$FePO_4$] framework. The electrode $FePO_4 \cdot 2H_2O$ material inserts 0.7 Li ions per mole leading to coulombic efficiency of 74% for the first cycle and specific capacity of 106 mAh g^{-1}. Infrared spectrum of the lithiated product shows structural modifications due to the lithium insertion and the reduction of iron ions.

Keywords: Iron phosphate; Lithium batteries; Raman; FTIR

1. Introduction

The phosphates of transition metals $M_y(PO_4)_z$ (with A = alkali, M = transition metal) form a wide family of compounds showing interesting properties which have engendered their potential-use as catalysts for selective oxidation reactions, being particularly effective for oxidative dehydrogenation [1], as positive electrodes for lithium batteries [2,3]. Among the huge family of compounds constituted by $(P_nO_{3n+1})^{(n+2)-}$ polyanions, the polyphosphates can be subclassified into (1) orthophosphates ($n = 1$) characterized by $(PO_4)^{3-}$ isolated units, (2) pyro- and diphosphates ($n = 2$) in which P_2O_7 groups are formed by two shared corner $(PO_4)^{3-}$ units, and (3) triphosphates ($n = 3$) where three $(PO_4)^{3-}$ units form $(P_3O_{10})^{5-}$ anions. The adaptability of PO_4 tetrahedra and P_2O_7 groups of interest possess an $M_y(PO_4)_z$ framework that houses interstitial Li^+ ions.

Since the pioneering work of Padhi et al. [4], mixed orthophosphates $LiMPO_4$ (M = Fe, Co, Ni, Mn) isostructural to olivine are intensively studied as lithium insertion compounds for Li batteries. Combined with discharge voltage between 3.4 and 4.8 V versus Li/Li^+, $LiFePO_4$ leads to high specific energy 150 mAh g^{-1} [3]. The generation of an appropriately high voltage is due to the presence of the polyanion $(PO_4)^{3-}$ with strong P–O covalency which stabilizes the antibonding Fe^{2+}/Fe^{3+} state through an Fe–O–P inductive effect. The inductive effect may be described as the action of one group to affect the electrostatically the electron distribution in other group. Thus, a change in distribution of the electrons modifies the force constant of the chemical bonds.

Iron phosphate, $FePO_4$, exists with different crystalline modifications as shown in Table 1 [5–8]. At normal pressures, $FePO_4$ adopts the verlinite structure related to the low-temperature α-quartz form [5]. The existence of several crystalline iron-phosphate phases was reported in the literature: the orthorhombic heterosite $FePO_4$ obtained from delithiated $LiFePO_4$ [3], the monoclinic $FePO_4$, and the orthorhombic $FePO_4$ [6]. Hydrated phases include the phosphosiderite (or metastrengite) $FePO_4 \cdot 2H_2O$ monoclinic form and the $FePO_4 \cdot 2H_2O$ orthorhombic form. Anhydrous iron pyrophosphate $Fe_4(P_2O_7)_3$ crystallizes in the orthorhombic system [9]. The schematic representation of the monoclinic structure of $FePO_4 \cdot 2H_2O$ is shown in Fig. 1. Moreover, it is

* Corresponding author. Tel.: +1 450 652 8019; fax: +1 450 652 8424.
E-mail address: karimz@ireq.ca (K. Zaghib).

0378-7753/$ – see front matter © 2004 Elsevier B.V. All rights reserved.
doi:10.1016/j.jpowsour.2004.09.042

Table 1
Crystal chemistry of the different crystalline modifications of iron phosphate

Compound	Space group	Crystallographic parameters				Ref.
		a (Å)	*b* (Å)	*c* (Å)	*β* (°)	
α-$FePO_4$ quartz	*P*321	5.033	5.033	11.247	–	[5]
Heterosite $FePO_4$	*Pnma*	9.8142	5.789	4.7820	–	[3]
Monoclinic $FePO_4$	$P2_1/n$	5.3071	9.7548	8.6752	90.16	[6]
Orthorhombic $FePO_4$	*Pbca*	9.8674	10.0973	8.7046	–	[6]
Monoclinic $FePO_4{\cdot}2H_2O$	$P2_1/n$	5.3125	9.7652	8.6837	90.44	This work
Orthorhombic $FePO_4{\cdot}2H_2O$	*Pbca*	9.1708	9.4564	8.6753	–	[6]
$Fe_4(P_2O_7)_3$	*Pbnm*	9.5622	21.5091	7.5451	–	[9]

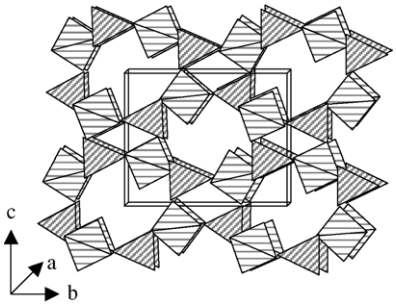

Fig. 1. Schematic representation of the monoclinic structure of $FePO_4{\cdot}2H_2O$.

obvious that hydrated $FePO_4$ is not competitive with $LiFePO_4$ as a cathode material for a Li^+-ion battery. The former compound exhibits a theoretical capacity of 143 mAh g^{-1} and an average discharge voltage of 2.7 V, while the olivine phase displays a wide voltage plateau at 3.5 V and a theoretical capacity of 170 mAh g^{-1}.

However, it is interesting to investigate the structural properties and electrochemical insertion reaction of the hydrate form of $FePO_4$. As previously reported for $MnO_2{\cdot}xH_2O$ [10] and $MoO_3{\cdot}xH_2O$ [11], the presence of structural water in these compounds can be beneficial for their electrochemical features. In this paper, we report the structural properties studied using X-ray diffractometry and vibrational spectroscopy (Raman and FTIR). The electrochemical behavior and the evolution of the structure upon lithium insertion in the $FePO_4{\cdot}2H_2O$ host material are also presented.

2. Experimental

$FePO_4{\cdot}2H_2O$ was hydrothermally synthesized from a mixture of $FeCl_2$, LiCl and H_3PO_4 in distilled water. Powder diffraction patterns were obtained on a Philips X'Pert-MPD diffractometer equipped with a solid-state detector and a Cu Kα radiation (λ = 1.5406 Å) source. The diffraction patterns were taken at room temperature in the range of $5^\circ < 2\theta < 80^\circ$ using step scans. The morphologies of the sample particles were examined by scanning electron microscopy using a Hitachi S-570 apparatus.

Raman spectra were recorded on a Jobin-Yvon U1000 double monochromator using the 514.5 nm line from a Spectra-Physics 2020 argon-ion laser. Standard photon-counting techniques were used for detection. In a typical spectral acquisition, six RS spectra each recorded with a resolution of 2 cm^{-1} were averaged to increase the signal-to-noise ratio. Infrared absorption spectra were recorded using a Bruker IFS113v vacuum FTIR interferometer. Samples were ground to fine powders, mixed approximately 1:300 with ICs, and vacuum pressed into translucent disks. In the far-infrared region (400–50 cm^{-1}), the vacuum bench apparatus was equipped with a 3.5-μm thick Mylar beam splitter, a globar source, and a liquid helium cooled bolometer. Samples were ground to fine powders and coated over solid-paraffin slab, which is a non-absorbing medium in the wavenumber range studied.

Electrochemical measurements were carried out using a Macpile potentiostat in the galvanostatic mode in the potential range 4–2 V at current density 7.23 mA g^{-1} (C/12 rate). The negative electrode was a disk of lithium metal foil. A Whattman borosilicate glass fiber sheet, saturated with a 1 M $LiPF_6$ salt dissolved in 1:1 EC/DMC solution, was placed between the two electrodes.

3. Results and discussion

3.1. Structure and morphology

Fig. 2 shows the XRD patterns of the phosphosiderite $FePO_4{\cdot}2H_2O$ powders. The diffractogram is dominated by two Bragg lines located at 19.1 and 20.2°. The XRD patterns were indexed by a monoclinic elementary cell with

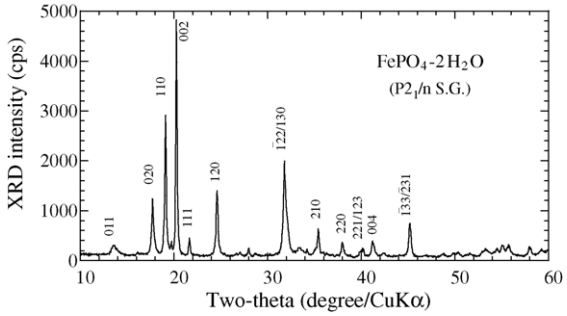

Fig. 2. XRD patterns of monoclinic $FePO_4{\cdot}2H_2O$.

space group $P2_1/n$. The $h\,k\,l$ values indexed for the diffraction lines are shown in Fig. 2. The lattice parameters refined in the monoclinic system are $a = 5.3125(6)$ Å, $b = 9.765(2)$ Å, $c = 8.683(7)$ Å and $\beta = 90°44'$. These values are in good agreement with those reported by Blanchard [12]. The lattice parameters are found to be slightly smaller than those of the metastrengite reported by Rémy and Boullé [13].

The crystallographic structure of monoclinic has been reported by Song et al. [6]. The structure of the phosphosiderite is built up from PO_4 tetrahedral and FeO_6 octahedra sharing corners to form three-dimensional framework (Fig. 1). This structure consists in a slight monoclinic distortion of the orthorhombic strengite-like framework. Each Fe octahedron share corners with four P tetrahedra, and the remaining two corners are occupied by two water molecules. Each PO_4 tetrahedron, in its turn, shares four corners with four FeO_6 octahedra.

Surface morphology and texture as well as particle size were observed by scanning electron microscopy. Fig. 3a–d shows typical SEM pictures of $FePO_4{\cdot}2H_2O$ powders (with various magnifications). It can be seen that the narrow particles in the sample are highly regular. Either size or the form of the particles is even. It can be explained by the high crystallinity and the absence of defects in the crystallites. Most of the particles have regular elongated shape and their dimensions are submicron-sized, i.e. the grain size average is around 800 nm. The SEM micrographs of $FePO_4{\cdot}2H_2O$ show a rather homogeneous size distribution of the nanoparticles. Since electrochemical lithium intercalation and deintercalation are in general limited by the rate of diffusion, the aforementioned features are important since smaller grain size can favor the lithium-ion mobility in the particles by reducing the ion-diffusion pathway.

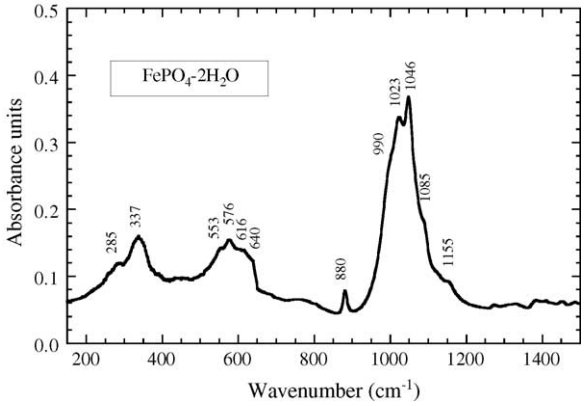

Fig. 4. FTIR absorption spectrum of $FePO_4{\cdot}2H_2O$.

3.2. Lattice dynamics

Figs. 4 and 5 show the FTIR absorption and Raman spectrum, respectively, of phosphosiderite $FePO_4{\cdot}2H_2O$. The vibrational motions of $FePO_4{\cdot}2H_2O$ may be divided into three classes: the stretching and bending vibrations of water molecules identified, respectively, around 3400 and 1610 cm^{-1}, the internal vibrations of $FePO_4$ located in the range 1200–400 cm^{-1} and external optical modes of $FePO_4$ situated below 400 cm^{-1}. It is worth mentioning that the

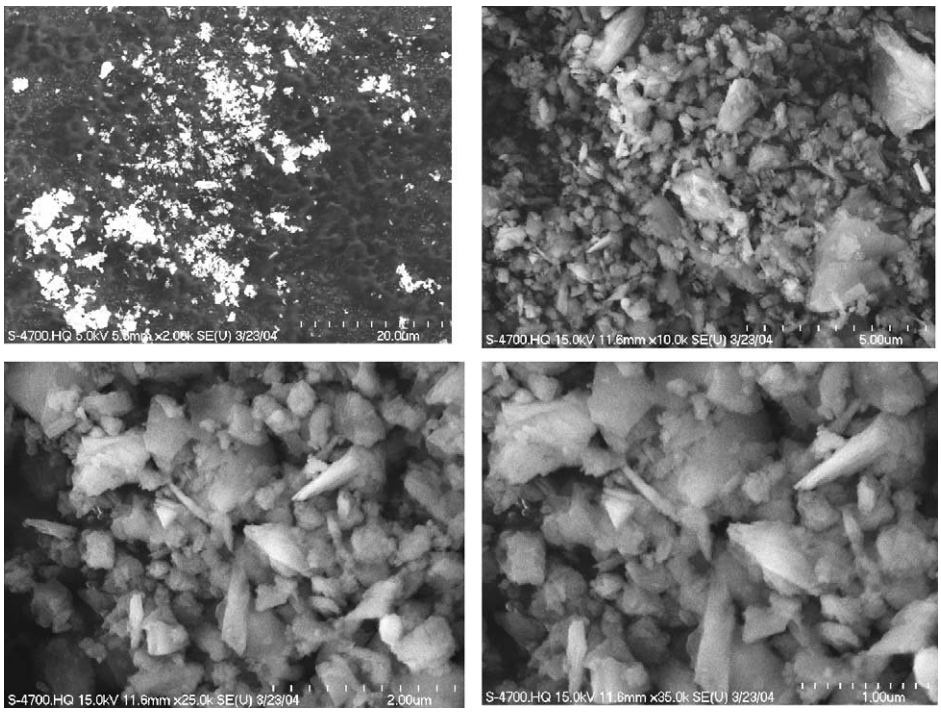

Fig. 3. SEM images of $FePO_4{\cdot}2H_2O$ (various magnifications).

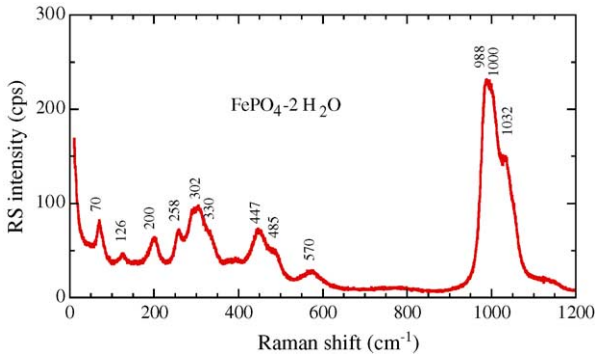

Fig. 5. Raman scattering spectrum of $FePO_4{\cdot}2H_2O$.

stretching (ν_{OH}) and bending (δ_{OH}) vibrations of water molecules are solely observed in infrared. In $FePO_4{\cdot}2H_2O$, the internal modes originate in the intramolecular vibrations of PO_4^{3-} anion. Fortunately, the bands originating in the intramolecular stretching motions of the phosphate anion (ν_3 and ν_1) can be assigned with confidence because they are highly decoupled while assignment of the bending modes (ν_4 and ν_2) makes problem because they are strongly coupled and involve some iron-ion motion.

Vibrational modes of tetrahedral XY_4 molecules are well known [14,15]. In order to facilitate the analysis of the vibrational spectra, we performed a factor group analysis for the internal and external vibrations of the PO_4 groups in phosphosiderite lattice, correlating the point group of the "free" ion (T_d) with its site group (C_i) and the factor group (C_{2h}). The results for the PO_4^{3-} units are shown in Table 2. Subtracting the three acoustic modes from the total number of vibrations, the optical modes are represented by

$$\Gamma = 12A_g + 12B_g + 9A_u + 9B_u \quad (1)$$

in which even (gerade) species are Raman-active and odd (ungerade) species are infrared-active modes.

Internal modes involve the displacement of oxygen atoms of the tetrahedral PO_4^{3-} anions and present frequencies closely related to those of the free molecule (in solution, for instance) with perfect T_d symmetry. For PO_4^{3-}, these are a singlet (A_1) at a frequency $\nu_1 = 938\,cm^{-1}$; a doublet (E) at $\nu_2 = 465\,cm^{-1}$ and two triply degenerate (F_2) modes, ν_3 at $1027\,cm^{-1}$ and ν_4 at $567\,cm^{-1}$. ν_1 and ν_3 involve the symmetric and antisymmetric stretching mode of the P–O bonds, whereas ν_2 and ν_4 involve mainly O–P–O symmetric and antisymmetric bending mode with a small contribution of P vibration [15]. In the solid $FePO_4{\cdot}2H_2O$, internal modes can split as a consequence of two effects: the site-symmetry effect due to an electric crystal field of symmetry lower than tetrahedral acting on the molecule and the correlation effect due to the presence of more than one molecular group in the crystal unit cell. Thus, we observe a frequency shift of the internal mode of PO_4 groups and a multiplicity of the fundamental modes due to the correlation $T_d \rightarrow C_{2h}$.

Table 2
Factor group analysis for $FePO_4$ in C_{2h}^5 symmetry

Atom	Site	A_g	A_u	B_g	B_u
Translations of Li, Fe, PO_4: 16 modes					
Fe	C_i	2	3	2	2
P	C_i	2	2	2	2
Librations of PO_4: 8 modes					
T_d	Site C_i			Correlation to D_{2h}	
F_1	$2A_g + 2A_g$			$2A_g + 2B_g + 2A_u + 2B_u$	
T_d	Site C_i			Correlation to D_{2h}	
Internal modes of PO_4: 20 modes					
$\nu_1(A_1)$	A_g			$A_g + B_g$	
$\nu_2(E)$	A_g			$A_g + B_g$	
$\nu_3(F_2)$	$2A_g + 2A_g$			$2A_g + 2B_g + 2A_u + 2B_u$	
$\nu_4(F_2)$	$2A_g + 2A_g$			$2A_g + 2B_g + 2A_u + 2B_u$	

As expected, the vibrational spectra (Figs. 4 and 5) are dominated by the fundamental vibrations of the PO_4^{3-} polyanions which are split in many components due to the correlation effect induced by the coupling with of Fe–O units in the structure. In the region of the internal modes of the phosphate anion (high-wavenumber region), we identify the symmetric stretching mode at $\nu_1 = 990\,cm^{-1}$; the doublet at $\nu_2 = 447$–$485\,cm^{-1}$; and the triplets ν_3 at 1000–1085 cm^{-1} and the triplet ν_4 in the region 570–640 cm^{-1}. A remarkable aspect of the Raman spectrum is the fact that both bending vibrations (ν_2 and ν_4) show reverse behavior, although usually the symmetric bending is expected to have a higher intensity. For condensed phosphates, the intensity of P–O stretching Raman bands near $1000\,cm^{-1}$ are always greater than those near $880\,cm^{-1}$, assigned to the stretching vibration ν_{P-O-P} of P–O–P bridges. Spectroscopic data giving the vibrational features of the monoclinic $FePO_4{\cdot}2H_2O$ are summarized in Table 3.

3.3. Lithium insertion

The electrochemical features of the monoclinic $FePO_4{\cdot}2H_2O$ positive electrode were examined using Li//$FePO_4{\cdot}2H_2O$ cells subjected to constant current cycling. The results from the electrochemical Li//$FePO_4{\cdot}2H_2O$ cell are presented as plot of cell voltage versus capacity (Fig. 6) as well as curve of the inverse derivative $-(\partial x/\partial V)$ versus cell voltage (Fig. 7). Plateaus in voltage versus capacity give rise to peaks in $-(\partial x/\partial V)$; so derivative plots are useful for displaying details.

Fig. 6 shows the first discharge–charge curve of the Li//$FePO_4{\cdot}2H_2O$ cell under galvanostatic conditions at 22 °C. The cells were charged and discharged at current densities of $0.5\,mA\,cm^{-2}$, while the voltage is monitored between 2.0 and 4.0 V. The coulombic efficiency of the first cycle was 74% (with a theoretical capacity $143\,mAh\,g^{-1}$) and the reversible capacity $106\,mAh\,g^{-1}$ is reached this time. The end of discharge the monoclinic $FePO_4{\cdot}2H_2O$ incorporates 0.7 Li per $FePO_4$. From the variation of the cell potential

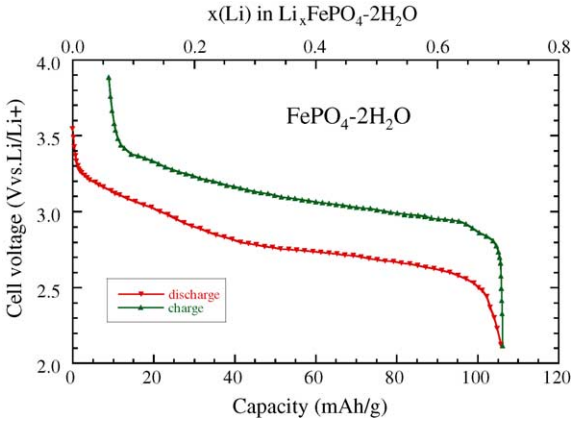

Fig. 6. Discharge–charge curve of the Li//$FePO_4 \cdot 2H_2O$ cell.

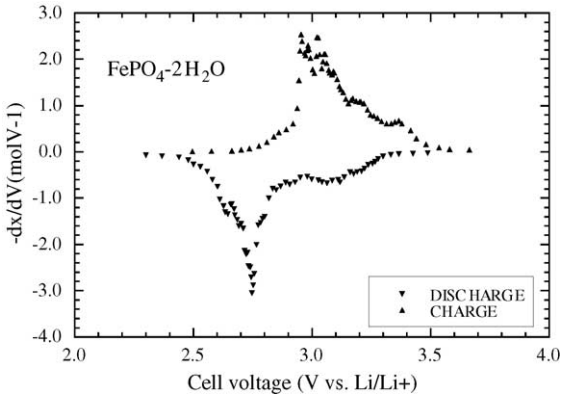

Fig. 7. Incremental capacity vs. cell voltage for the first cycle of the Li//$FePO_4 \cdot 2H_2O$ cell.

for the complete cell (Fig. 6), one can see the presence of two regions during the lithium insertion processes. The first discharge profile exhibits a rapid decay of the voltage in the range 3.5–2.8 V with a slope 1.7 V mol^{-1} followed by a pseudo-plateau in the range 2.8–2.6 (slope 0.5 V mol^{-1}). These two regimes appear also in the charge curve. Note that the average voltage of $FePO_4 \cdot 2H_2O$ is much smaller than that of the $LiFePO_4$ olivine structure which displays a plateau at 3.5 V.

Fig. 7 displays the incremental capacity versus cell voltage for the first cycle of the Li//$FePO_4 \cdot 2H_2O$ cell. The reduction peak occurs at 2.75 V while the oxidation reaction is centered at 3.0 V. The two regimes of intercalation are clearly depicted when derivative voltage $-(\partial x/\partial V)$ is plotted versus cell voltage. The broad band centered at 3.05 V (capacity around $x = 0.12$) is indicative of the one-phase system, while the narrow band at 3.74 V (capacity around 0.52) is indicative of the two-phase system.

Table 3
Observed FTIR and Raman bands in $FePO_4 \cdot 2H_2O$

Frequency (cm^{-1})		Assignment
FTIR	Raman	
480		ν(OH)
3370		ν(OH)
1610		δ(OH)
1155		$\nu_{P—O—P}$
1085		ν_3
1046	1032	ν_3
1023	1000	ν_3
990	988	ν_1
880		$\nu_{P—O—P}$
640		ν_4
616		ν_4
576	570	ν_4
553		ν_4
	485	ν_2
	447	ν_2
337	330	
285	302	Lattice
	258	Modes
	128	
	70	

Fig. 8 displays the FTIR spectrum of lithiated $Li_{0.7}FePO_4 \cdot 2H_2O$ electrode recorded on material taken from a cell discharged at 2.5 V (end of discharge). This FTIR spectrum shows clearly the structural change that occurred in $FePO_4 \cdot 2H_2O$ upon Li insertion ($x = 0.7$). The lithiated product displays a spectrum with significant shift ($\Delta\nu = 11\ cm^{-1}$) of the stretching vibrations of the PO_4^{3-} groups and additional bands in the far-infrared region (below 500 cm^{-1}). These two effects are due to both the reduction of $Fe^{3+} \rightarrow Fe^{2+}$ and the presence of lithium in the channels of the [$FePO_4$] network. We observed the appearance of new IR bands at 495, 454 and 368 cm^{-1} which are attributed to the stretching and bending vibrations, respectively, of Li ions in an octahedral environment [16]. For the lithiated Li_xFePO_4 phase, the factor group theory predicts five ($3A_u + 2B_u$) extra infrared-active modes. Furthermore, the whole spectral features Li_xFePO_4 are consistent with the monoclinic C_{2h}^5 space group.

In this regard, it is interesting to compare the position of the Fe^{3+}/Fe^{2+} redox couple between the $LiFePO_4$ olivine

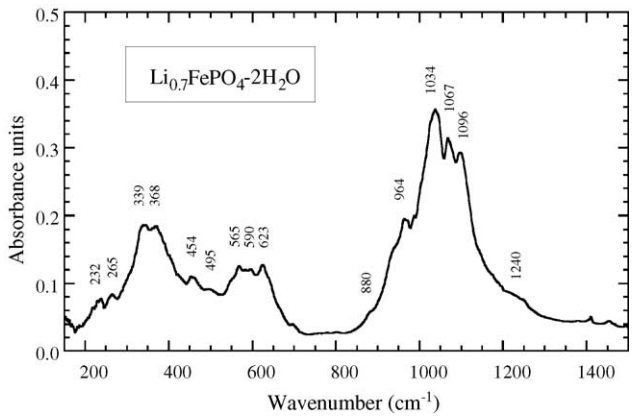

Fig. 8. FTIR spectrum of lithiated $Li_{0.7}FePO_4 \cdot 2H_2O$ electrode taken at the end of discharge.

structure and the hydrate $FePO_4$ phase (3.5 V versus 2.7 V). With the presence of structural water, the [$FePO_4$] network exhibits a weaker P–O covalency which can be viewed in the vibrational spectrum (frequency shift of the $\nu_3(PO_4)$-like modes); thus the Fe–O–P inductive effect is less effective. $FePO_4{\cdot}2H_2O$ heated at 650 °C, we obtained $FePO_4$ without the presence of structural water, this compound is an excellent precursor for $LiFePO_4$ synthesis.

4. Conclusion

In this work, we have studied the structural and electrochemical properties of the hydrate form of $FePO_4$. The structural properties investigated using X-ray diffractometry shows the monoclinic structure of $FePO_4{\cdot}2H_2O$ ($P2_1/n$ space group). Lattice dynamics studied by Raman and FTIR spectroscopy show the strong inductive effect in the [$FePO_4$] framework. The electrochemical features of the monoclinic $FePO_4{\cdot}2H_2O$ positive electrode were evaluated by examining the discharge–charge curve and the inverse derivative $-(\partial x/\partial V)$ versus cell voltage. The electrode $FePO_4{\cdot}2H_2O$ material inserts by 0.7 Li ions per mole and leading to a specific capacity of 106 mAh g^{-1}. Infrared spectrum of the lithiated product shows structural modifications due to the Li insertion and the reduction of Fe^{3+} ions.

References

[1] M. Ai, K. Ohdan, J. Mol. Catal. A: Chem. 159 (2000) 19.
[2] A. Manthiram, J.B. Goodenough, J. Power Sources 26 (1989) 403.
[3] A.S. Andersson, B. Kalska, L. Haggstrom, J.O. Thomas, Solid State Ionics 130 (2000) 41.
[4] A.K. Padhi, K.S. Nanjundaswamy, J.B. Goodenough, J. Electrochem. Soc. 144 (1997) 1188.
[5] H.N. Nang, C. Calvo, Can. J. Chem. 53 (1975) 2064.
[6] Y. Song, P.Y. Zavalij, M. Suzuki, M.S. Whittingham, Inorg. Chem. 41 (2002) 5778.
[7] C. Masquelier, P. Reale, C. Wurm, M. Morcrette, L. Dupont, D. Larcher, J. Electrochem. Soc. 149 (2002) 1037.
[8] M. Cavellec, D. Riou, G. Ferey, Inorg. Chim. Acta 291 (1999) 317.
[9] K.K. Palkina, S.I. Maksimova, S.I. Chibiskova, K. Schlesinger, G. Ladig, Z. Anorg. Allg. Chem. 529 (1985) 89.
[10] S. Bach, J.P. Pereira-Ramos, N. Baffier, Solid State Ionics 80 (1995) 151.
[11] C. Guzman, B. Yebka, J. Livage, C. Julien, Solid State Ionics 86–88 (1996) 407.
[12] F. Blanchard, ASTM Card 33-0666, 1981.
[13] P. Rémy, A. Boullé, CR Acad. Sci. Paris 253 (1961) 2699.
[14] W.G. Fateley, F.R. Dollish, N.T. McDevitt, F.F. Bentley, Infrared and Raman Selection Rules for Molecular and Lattice Vibrations: The Correlation Method, Wiley, New York, 1972.
[15] K. Nakamoto, Infrared and Raman Spectra of Inorganic and Coordination Compounds, Wiley, New York, 1978.
[16] C. Julien, Ionics 6 (2000) 30.